Surface-Enhanced Nonlinear Four-Wave Mixing

Jan Renger,[1] Romain Quidant,[1] Niek van Hulst,[1] and Lukas Novotny[1,2]

[1]*ICFO-Institut de Ciencies Fotoniques, Mediterranean Technology Park, 08860 Castelldefels (Barcelona), Spain*

[2]*The Institute of Optics, University of Rochester, Rochester, New York 14627, USA*

(Received 17 November 2009; revised manuscript received 4 January 2010; published 29 January 2010; publisher error corrected 2 February 2010)

We report on a particularly strong third-order nonlinear response from nanostructured gold surfaces. Two incident laser beams with frequencies ω_1 and ω_2 give rise to four-wave mixing (4WM) fields with frequencies $2\omega_1 - \omega_2$ and $2\omega_2 - \omega_1$. We demonstrate that the nonlinear response can be purely evanescent and that nanostructured surfaces convert the evanescent energy into propagating radiation, thereby increasing the efficiency of frequency conversion. The emitted 4WM radiation is found to be directional, polarized, coherent, and both frequency and angle tunable. The ability to perform efficient frequency conversion in reduced dimensions provides new opportunities for nanophotonics and active plasmonics.

DOI: 10.1103/PhysRevLett.104.046803 PACS numbers: 73.20.Mf, 42.65.Ky, 78.47.nj, 78.68.+m

Efficient optical frequency conversion requires the nonlinear response from individual atoms or molecules to be summed up coherently, a process referred to as phase matching [1]. This task is typically accomplished in nonlinear crystals many wavelengths in size. However, various applications in nanophotonics (e.g., logic, switching, sensing) require frequency conversion in materials with reduced dimensions, such as interfaces [2–5] or discrete particles [6–8]. A strong *local* nonlinear response relies on intrinsic material parameters and on the particular material geometry [9].

While second-order nonlinear processes, such as second-harmonic generation and sum-frequency generation, have been extensively studied on surfaces and interfaces of various kinds [2,6,7,10,11], third-order processes have received considerably less attention. Here, we demonstrate very efficient third-order nonlinear frequency mixing at nanostructured gold surfaces and show that the nonlinear process can be controlled and manipulated at the nanometer scale. We find that the fields at the nonlinear frequency can be purely evanescent, allowing all the nonlinear energy to be concentrated at the very surface, thereby suppressing radiation losses.

To quantitatively understand the third-order nonlinear response of metals, it is necessary to perform experiments on well characterized structures. The planar geometry is particularly simple and makes it possible to achieve a coherent and directional response. However, the nonlinear response also depends on the ability to couple radiation into and out of the material. We demonstrate that the coupling efficiency can be strongly enhanced by surface nanostructuring. We perform quantitative optical four-wave mixing (4WM) experiments on planar and nanostructured gold surfaces and demonstrate highly directional and tunable emission.

Figure 1 illustrates the experimental arrangement. Two coherent laser beams with center frequencies ω_1 and ω_2 are incident from angles θ_1 and θ_2, respectively, on a nanostructured gold surface. The angles are measured from the surface normal in clockwise direction. The two beams induce a nonlinear polarization at frequencies

$$\omega_{4\mathrm{wm}_1} = 2\omega_1 - \omega_2 \qquad \omega_{4\mathrm{wm}_2} = 2\omega_2 - \omega_1, \tag{1}$$

which in turn give rise to two outgoing beams propagating at angles $\theta_{4\mathrm{wm}_1}$ and $\theta_{4\mathrm{wm}_2}$, respectively. The two nonlinear processes can be expressed by a nonlinear polarization according to

$$\begin{aligned} \mathbf{P}^{(1)} &= \varepsilon_0 \chi^{(3)}(-\omega_{4\mathrm{wm}_1}; \omega_1, \omega_1, -\omega_2)\mathbf{E}_1\mathbf{E}_1\mathbf{E}_2^* \\ \mathbf{P}^{(2)} &= \varepsilon_0 \chi^{(3)}(-\omega_{4\mathrm{wm}_2}; \omega_2, \omega_2, -\omega_1)\mathbf{E}_1\mathbf{E}_1\mathbf{E}_2^*, \end{aligned} \tag{2}$$

where $\mathbf{E}_i$ are the electric field vectors associated with the incident beams of frequencies ω_i, and $\chi^{(3)}$ is the third-order surface susceptibility, a tensor of rank four. The

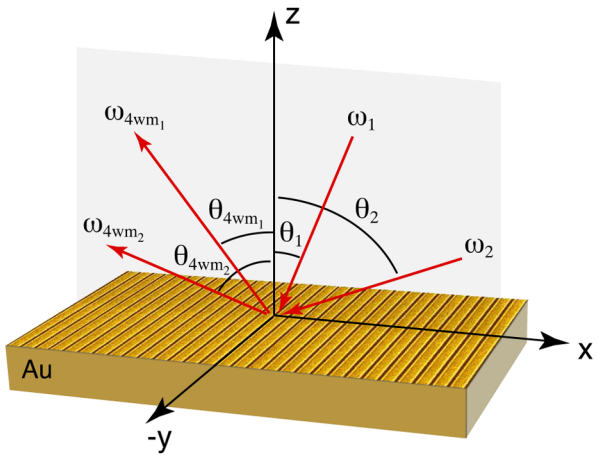

FIG. 1 (color online). Nonlinear four-wave mixing at a nanostructured gold surface. Two incident laser beams with frequencies ω_1 and ω_2 give rise to reflected beams with frequencies $\omega_{4\mathrm{wm}_1} = 2\omega_1 - \omega_2$ and $\omega_{4\mathrm{wm}_2} = 2\omega_2 - \omega_1$, respectively.

volume that contributes to the nonlinear response is determined by the penetration depth into the metal, which can be influenced by surface nanostructuring. However, to establish a theoretical understanding and for later reference, we will first consider a planar surface.

Equations (1) are statements of energy conservation. They define the frequencies of the outgoing radiation. Similarly, momentum conservation defines the outgoing propagation directions according to

$$\begin{aligned}\omega_{4\mathrm{wm}_1}\sin\theta_{4\mathrm{wm}_1} &= \omega_2\sin\theta_2 - 2\omega_1\sin\theta_1\\ \omega_{4\mathrm{wm}_2}\sin\theta_{4\mathrm{wm}_2} &= \omega_1\sin\theta_1 - 2\omega_2\sin\theta_2.\end{aligned} \tag{3}$$

After substituting Eqs. (1), it becomes evident, that *real* solutions for $\theta_{4\mathrm{wm}_1}$ and $\theta_{4\mathrm{wm}_2}$ exist only for certain angular ranges of θ_1 and θ_2. *Imaginary* solutions represent surface-bound, evanescent 4WM fields.

Using the coordinate system defined in Fig. 1, each of the fields $\mathbf{E}_i$ in Eq. (2) can be represented in terms of the angle of incidence θ_i, polarization angle ϕ_i, and wave vector $\mathbf{k}_i = (-k_i\sin\theta_i, 0, k_i\cos\theta_i)$ as

$$\mathbf{E}_i = E_i^0\begin{bmatrix}-\cos\theta_i\sin\phi_i t_p(\theta_i)\\ \cos\phi_i t_s(\theta_i)\\ \sin\theta_i\sin\phi_i t_p(\theta_i)\end{bmatrix}e^{i[\mathbf{k}_i\cdot\mathbf{r}-\omega_i t]} \tag{4}$$

where t_s and t_p are the Fresnel transmission coefficients for s and p polarized incident light, respectively, and E_i^0 is the amplitude of the incident field. We next assume that the nonlinear response is associated with the bulk and that the material is isotropic. In this case, the 81 components of $\chi^{(3)}$ can be reduced to only three nonzero and independent components [1], namely $\chi^{(3)}_{1212}$, $\chi^{(3)}_{1221}$, and $\chi^{(3)}_{1122}$. Here, the indices "1" and "2" stand for any Cartesian index (x, y, or z), with the condition that $'1' \neq '2'$. The only other nonzero components are $\chi^{(3)}_{1111} = [\chi^{(3)}_{1212} + \chi^{(3)}_{1221} + \chi^{(3)}_{1122}]$. For the case of four-wave mixing considered here, two of the incident fields are identical [c.f. Eq. (2)] and hence $\chi^{(3)}_{1212} = \chi^{(3)}_{1122}$. The two remaining components, together with the input fields E_1^0 and E_2^0, define the nonlinear polarization, which can be written as $\mathbf{P} = [P_x, P_y, P_z]^T \times \exp[i\mathbf{k}_{4\mathrm{wm}}\cdot\mathbf{r} - i\omega_{4\mathrm{wm}}t]$, where $\mathbf{k}_{4\mathrm{wm}} = 2\mathbf{k}_1 - \mathbf{k}_2$ or $\mathbf{k}_{4\mathrm{wm}} = 2\mathbf{k}_2 - \mathbf{k}_1$, depending on which of the two four-wave mixing processes is being dealt with.

The nonlinear polarization $\mathbf{P}$ defines a source current and gives rise to electromagnetic fields at the four-wave mixing frequency $\omega_{4\mathrm{wm}}$. The nonlinear field $\mathbf{E}_{4\mathrm{wm}}$ can be calculated as [12]

$$\mathbf{E}_{4\mathrm{wm}} = \frac{1}{\varepsilon_0}\left[\frac{k_{4\mathrm{wm},z} - k_{\downarrow,z}}{k_\downarrow^2 - k_{4\mathrm{wm}}^2}\right]e^{i[\mathbf{k}_\uparrow\cdot\mathbf{r}-\omega_{4\mathrm{wm}}t]}\begin{bmatrix}k_{\uparrow,z}(k_{\downarrow,z}P_x + k_{\downarrow,x}P_z)/[\varepsilon k_{\uparrow,z} - k_{\downarrow,z}]\\ -k_\downarrow^2 P_y/[\varepsilon(k_{\uparrow,z} - k_{\downarrow,z})]\\ -k_{\uparrow,x}(k_{\downarrow,z}P_x + k_{\downarrow,x}P_z)/[\varepsilon k_{\uparrow,z} - k_{\downarrow,z}]\end{bmatrix}. \tag{5}$$

Here, $k_\uparrow^2 = (\omega_{4\mathrm{wm}}/c)^2$ and $k_\downarrow^2 = \varepsilon(\omega_{4\mathrm{wm}}/c)^2$, with $\varepsilon = \varepsilon(\omega_{4\mathrm{wm}})$. Because of momentum conservation along the interface, $k_{4\mathrm{wm},x} = k_{\downarrow,x} = k_{\uparrow,x}$. Depending on which of the two four-wave mixing processes is being considered, we further have $k_{4\mathrm{wm},x} = 2k_{1,x} - k_{2,x}$ or $k_{4\mathrm{wm},x} = 2k_{2,x} - k_{1,x}$, which is a restatement of Eq. (3). Furthermore, since $k_{1,y} = k_{2,y} = 0$ for the incident waves, we also have $k_{4\mathrm{wm},y} = k_{\downarrow,y} = k_{\uparrow,y} = 0$.

We are now able to express the field $\mathbf{E}_{4\mathrm{wm}}(\omega_{4\mathrm{wm}})$ in terms of the incident fields $E_1^0(\omega_1)$ and $E_2^0(\omega_2)$ and the two independent third-order susceptibility components $\chi^{(3)}_{1212}$ and $\chi^{(3)}_{1221}$. All fields E_i^0 are related to the corresponding laser peak powers $\hat{P}_i$ by $E_i^0 = [2\hat{P}_i/(\varepsilon_0 c A_i)]^{1/2}$, where A_i are the spot areas. Using the here outlined theory together with the experimental values for the input powers (P_1, P_2) and output powers ($P_{4\mathrm{wm}}$), we determine a value of $\chi^{(3)} = 0.2\ \mathrm{nm}^2/\mathrm{V}^2$ for the magnitude of the third-order nonlinear susceptibility of gold [13], which is more than 2 orders of magnitude larger than the value of $LiNbO_3$ [14].

The choice of the excitation angles θ_1 and θ_2 does not only define the directions $\theta_{4\mathrm{wm}_i}$ of the emitted 4WM radiation but it also strongly influences the efficiency of the 4WM process. In Fig. 2(a), we plot $|\mathbf{E}_{4\mathrm{wm}}(\theta_1, \theta_2)|^2$ for p-polarized ($\phi = 0$) input fields of equal amplitude and for $\lambda_{4\mathrm{wm}_1} = 633$ nm. The wavelengths of the excitation lasers are $\lambda_1 = 707$ nm and $\lambda_2 = 800$ nm, respectively. We

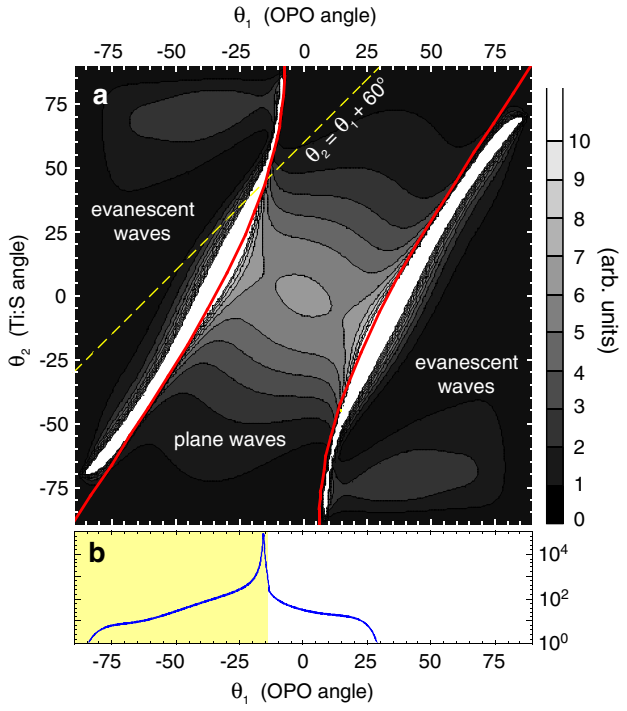

FIG. 2 (color online). (a) Efficiency of four-wave mixing ($|\mathbf{E}_{4\mathrm{wm}}|^2$) at $\lambda_{4\mathrm{wm}_1} = 633$ nm as a function of excitation angles θ_1 and θ_2. The solid line indicates the boundary between propagating and evanescent 4WM waves. (b) Line cut along the dashed line. The shaded area corresponds to the evanescent region. The intensity at the surface plasmon peak is more than 3 orders of magnitude larger than the intensity in the propagating region.

have used $\chi^{(3)}_{1221}/\chi^{(3)}_{1212} = 4$, as determined from independent polarization measurements. The contour plot reveals that the 4WM efficiency is strongly dependent on the excitation angles θ_1 and θ_2. The results for $\lambda_{4\mathrm{wm}_2} = 921$ nm are similar and are not reproduced here.

The solid curves in the figure denote the boundaries between *propagating* 4WM waves and *evanescent* 4WM waves. They correspond to the lines $k_{\uparrow,z} = 0$, where $k_{\uparrow,z}$ is the vertical component of the wave vector $\mathbf{k}_\uparrow$, calculated as

$$k_{\uparrow,z}(\omega_{4\mathrm{wm}_1}) = \sqrt{\frac{\omega^2_{4\mathrm{wm}_1}}{c^2} - k^2_{4\mathrm{wm}_1,x}}. \quad (6)$$

Here, according to Eq. (3), $k_{4\mathrm{wm}_1,x} = 2k_{1,x} - k_{2,x} = -[2(\omega_1/c)\sin\theta_1 - (\omega_2/c)\sin\theta_2]$.

The finding that the 4WM fields can be evanescent opens up the possibility of generating confined optical energy at the 4WM frequency locally, without coupling to radiative modes. Interestingly, the highest 4WM efficiency is found in the evanescent region, namely, where the evanescent 4WM wave couples to surface plasmon polaritons [c.f. Fig. 2(b)] [15].

In our experiments, we use a Ti:Sapphire laser providing pulses of duration ~200 fs and center wavelength $\lambda_2 = 800$ nm, and an optical parametric oscillator (OPO) providing pulses of similar duration and wavelength $\lambda_1 = 707$ nm. The beams are first expanded to 10 mm diameter and then focused by two lenses of focal length $f = 50$ mm on a gold surface with roughness 2.3 $\mathrm{nm_{rms}}$, as determined by atomic force microscopy. The angle between the two laser beams is held fixed at $\theta_2 - \theta_1 = 60°$, and the laser pulses are made to overlap in time by use of a delay line. The spot diameters at the surface are ~4.5 μm and are spatially overlapping. We use two different detection angles, which are both fixed with respect to the angles of the excitation beams, namely $\theta_{\mathrm{det}} = \theta_1 + 60°$ and $\theta_{\mathrm{det}} = \theta_1 + 26°$. The scattered radiation is collected by $f = 50$ mm lenses, filtered by optical stop-band filters to reject light at the excitation frequencies, and then sent into a fiber-coupled spectrometer.

Fixing the angle between the excitation beams to $\theta_2 - \theta_1 = 60°$ reduces the (θ_1, θ_2) parameter space to the dashed line in Fig. 2 and makes the 4WM propagation angles $\theta_{4\mathrm{wm}_1}$ and $\theta_{4\mathrm{wm}_2}$ functions of only one angle [c.f. Eq. (3)]. For $\lambda_1 = 707$ nm and $\lambda_2 = 800$ nm, the curves in Fig. 3(a) show the calculated angles of the 4WM radiation according to Eqs. (1) and (3). The figure reveals that propagating 4WM fields exist only for certain ranges of excitation angles. For other angles, the solutions are evanescent. Within the angular regions for which propagating 4WM waves exist, the direction of 4WM emission can be tuned by sample rotation.

According to the graphs in Fig. 3(a), to detect 4WM in direction of $\theta_{\mathrm{det}} = \theta_1 + 60°$, the incident angle needs to be adjusted to $\theta_1 = -5.4°$ for $\lambda_{4\mathrm{wm}_1} = 633$ nm and to $\theta_1 = -83.1°$ for $\lambda_{4\mathrm{wm}_2} = 921$ nm. To verify these predictions,

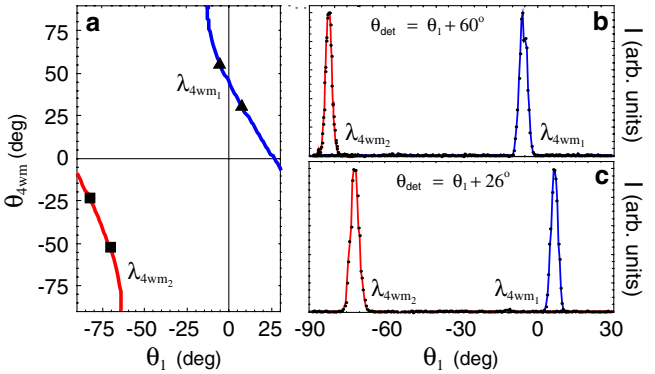

FIG. 3 (color online). Angular dependence of 4WM emission. (a) Calculated emission angles ($\theta_{4\mathrm{wm}_1}$, $\theta_{4\mathrm{wm}_2}$) as a function of excitation angle θ_1. The angle of θ_2 is $\theta_1 + 60°$. $\lambda_1 = 707$ nm, $\lambda_2 = 800$ nm, $\lambda_{4\mathrm{wm}_1} = 633$ nm, and $\lambda_{4\mathrm{wm}_2} = 921$ nm. (b), (c) Measured 4WM intensity as a function of excitation angle θ_1. The four resonance curves correspond to the angles marked by triangles and squares in (a).

we record the 4WM intensities as a function of sample rotation angle and calibrate against θ_1. Figure 3(b) shows the recorded angular dependence of the 4WM intensity using a detection angle of $\theta_{\mathrm{det}} = \theta_1 + 60°$. The measured peak values occur at $\theta_1 = -4.8°$ ($\lambda_{4\mathrm{wm}_1} = 633$ nm) and $\theta_1 = -82.8°$ ($\lambda_{4\mathrm{wm}_2} = 921$ nm), respectively. The slight deviation from the theoretically predicted values originates from calibration uncertainties and the angular dependence of the detection efficiency. The width of the peaks $\Delta\theta_1 \approx 4°$ originates from the fact that our excitation beams are not plane waves but focused beams with an angular range defined by the focusing lenses. Similar results were measured for other detection angles. Figure 3(c) shows the results for $\theta_{\mathrm{det}} = \theta_1 + 26°$. For this angle, we calculate that 4WM at $\lambda_{4\mathrm{wm}_1} = 633$ nm is possible for $\theta_1 = 6.2°$, and 4WM at $\lambda_{4\mathrm{wm}_2} = 921$ nm for $\theta_1 = -72.9°$. The measured peak positions are $\theta_1 = -7.2°$ and $\theta_1 = -72.8°$, respectively, which again is in excellent agreement with the predicted values.

According to Fig. 2, a considerable range of excitation angles (θ_1, θ_2) gives rise to evanescent 4WM fields. To extract the energy of evanescent 4WM waves, we nanostructured the gold surface with a grating of period a. The grating introduces an in-plane momentum of $\pm 2\pi/a$ and modifies the momentum conservation in Eq. (3) as

$$\begin{aligned} \omega_{4\mathrm{wm}_1}\sin\theta_{4\mathrm{wm}_1} &= \omega_2\sin\theta_2 - 2\omega_1\sin\theta_1 \pm n2\pi c/a \\ \omega_{4\mathrm{wm}_2}\sin\theta_{4\mathrm{wm}_2} &= \omega_1\sin\theta_1 - 2\omega_2\sin\theta_2 \pm n2\pi c/a, \end{aligned} \quad (7)$$

where n is the grating order. For 4WM at $\lambda_{4\mathrm{wm}_1} = 633$ nm, the largest in-plane wave vector $k_{4\mathrm{wm},x}$ along the dashed line in Fig. 2(a) is found near $\theta_1 = -60°$. The corresponding in-plane wavelength of the evanescent 4WM wave is $2\pi/k_{4\mathrm{wm},x} = 365$ nm. For outcoupling towards the detection direction $\theta_{\mathrm{det}} = \theta_1 + 26°$, we used electron beam

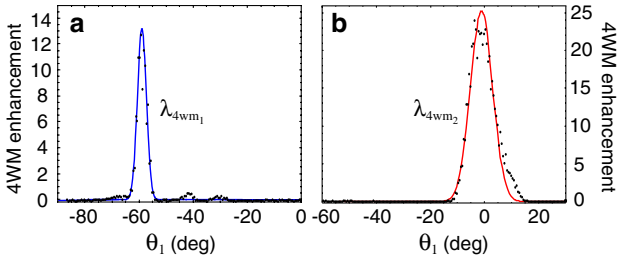

FIG. 4 (color online). Enhanced 4WM from nanostructured surfaces. (a) The 4WM intensity at $\lambda_{4wm_1} = 633$ nm as a function of excitation angle θ_1. A grating with period $a = 300$ nm is used to couple out evanescent 4WM fields with in-plane wavelength of 365 nm. (b) The 4WM intensity at $\lambda_{4wm_2} = 921$ nm as a function of excitation angle θ_1. A grating with period $a = 371$ nm is used to couple out evanescent 4WM fields with in-plane wavelength of 461 nm. Dots are data points, and the solid curves are a Gaussian fit. Data normalized with the 4WM intensity measured for a flat gold surface.

lithography and reactive ion etching to fabricate a first order ($n = 1$) grating with grooves of 70 nm depth, 100 nm width, and 300 nm period.

Figure 4(a) shows the measured 4WM intensity as a function of excitation angle θ_1. We find that the maximum 4WM intensity is enhanced by more than 1 order of magnitude relative to the maximum intensity obtained from a planar gold surface [at $\theta_1 = 6.9°$ in Fig. 3(c)]. This enhancement can be attributed to the enhanced fields at the nanostructured surface and the improved coupling efficiency. Notice that much higher enhancement factors can be expected for θ_1 near the surface plasmon peak [15] and for optimized grating geometries [16].

Similar measurements were performed for 4WM at $\lambda_{4wm_2} = 921$ nm using a grating with period $a = 371$ nm. The largest in-plane wave vector is calculated near $\theta_1 = 0°$. The measurements shown in Fig. 4(b) yield a peak centered at $\theta_1 = -1.5°$. As before, we find good agreement for the peak position and observe a 4WM efficiency enhancement of $\sim$25 over the planar gold surface. However, we also observe a significant broadening of the directionlity of 4WM emission. This broadening is due to deviations from the perfect grating geometry and fluctuations of the laser wavelengths. Small deviations in the grating period or the laser wavelengths yield relatively large changes in emission angle for this highly dispersive grating. This effect can be minimized by using gratings with slightly larger periodicity and by using more accurate fabrication procedures.

Our work demonstrates that a multiphoton process, such as four-wave-mixing, can be employed to vectorially add the in-plane momenta of incident photons in order to create propagating or evanescent waves. Surface nanostructuring makes it possible to convert evanescent 4WM waves into propagating radiation and to improve the in and outcoupling of radiation, thereby increasing the 4WM efficiency significantly. The nonlinear response can be further increased by exploiting local field enhancement at nanostructured surfaces. The emitted 4WM radiation is coherent, directional, and both frequency and angle tunable. The finding that freely propagating incident radiation can give rise to nonpropagating localized fields at a material's surface can be exploited for a broad range of applications, such as dark-field microscopy or the frequency-selective excitation of surface modes (surface plasmons polaritons, guided waveguide modes, surface phonon polaritons, etc.).

This research was funded by the National Science Foundation (ECCS-0918416), the Catalan AGAUR pivprogram, and ICREA. We thank Mark Kreuzer, Michael Yarrow (Radiantis), Bradley Deutsch, Stefano Palomba, Lars Neumann, and Srjan Acimovic for technical support and sample characterization.

[1] R. W. Boyd, *Nonlinear Optics* (Academic Press, San Diego, 2008), 3rd ed.
[2] F. Brown, R. E. Parks, and A. M. Sleeper, Phys. Rev. Lett. **14**, 1029 (1965).
[3] N. A. Papadogiannis, P. A. Loukakos, and S. D. Moustaizis, Opt. Commun. **166**, 133 (1999).
[4] B. Lamprecht, J. R. Krenn, A. Leitner, and F. R. Aussenegg, Phys. Rev. Lett. **83**, 4421 (1999).
[5] S. Palomba and L. Novotny, Phys. Rev. Lett. **101**, 056802 (2008).
[6] A. Leitner, Mol. Phys. **70**, 197 (1990).
[7] A. Bouhelier, M. Beversluis, A. Hartschuh, and L. Novotny, Phys. Rev. Lett. **90**, 013903 (2003).
[8] M. Lippitz, M. A. van Dijk, and M. Orrit, Nano Lett. **5**, 799 (2005).
[9] M. Danckwerts and L. Novotny, Phys. Rev. Lett. **98**, 026104 (2007).
[10] T. F. Heinz, *Nonlinear Surface Electromagnetic Phenomena*, edited by H. E. Panath and G. I. Stegeman (Elsevier, Amsterdam, 1991).
[11] H. B. Jiang *et al.*, Phys. Rev. B **44**, 1220 (1991).
[12] N. Bloembergen and P. S. Pershan, Phys. Rev. **128**, 606 (1962).
[13] N. Bloembergen, W. K. Burns, and M. Matsuoka, Opt. Commun. **1**, 195 (1969).
[14] R. A. Ganeev *et al.*, Opt. Commun. **229**, 403 (2004).
[15] J. Renger *et al.*, Phys. Rev. Lett. **103**, 266802 (2009).
[16] F. Lopez-Tejeira *et al.*, Nature Phys. **3**, 324 (2007).